Supplement of Hydrol. Earth Syst. Sci., 29, 3703–3725, 2025
https://doi.org/10.5194/hess-29-3703-2025-supplement

Hydrology and Earth System Sciences
Open Access
EGU

Supplement of

Predicting snow cover and frozen ground impacts on large basin runoff: developing appropriate model complexity

Nan Wu et al.

Correspondence to: Ke Zhang (kzhang@hhu.edu.cn)

1. Equations for evaluating model performance

The criteria for hydrological model simulation performance are defined as flows:

$$RMSE = \sqrt{\sum_{i=1}^{n} (X_s - X_o)^2 / n} \tag{S1}$$

$$BIAS = \sum_{i=1}^{n} (X_s - X_o) / n \tag{S2}$$

$$NSE = 1 - \sum_{i=1}^{n} (X_s - X_o)^2 \Big/ \sum_{i=1}^{n} (X_o - \overline{X_o})^2 \tag{S3}$$

$$RE = \left(\sum_{i=1}^{n} (X_s - X_o) \Big/ \sum_{i=1}^{n} X_o \right) \times 100\% \tag{S4}$$

where X_s represents the simulated values, X_o represents the observed values, $\overline{X_o}$ is the mean of the observed values, and n is the number of time series observations.

2. Implementation

Using the observed ground surface temperature data from six meteorological stations within the basin, the initial freezing and thawing dates of the frozen surface layer were determined and compared with the model simulation results, with missing data points from station 56158 for the period 2015-2018. As shown in Figure S6, the observed and simulated results were quite similar; the upstream stations (56034 and 56038) exhibited earlier freezing (October) and later thawing (April) compared to the four midstream stations. Additionally, all stations during the study period showed a trend of delayed onset of freezing and earlier onset of thawing. Although the number of stations is limited, the point-scale data provided strong validation for the simulated soil freeze-thaw processes.

In order to emphasize the role of seasonal snowmelt in the annual hydrological cycle, the monthly rainfall, snowmelt and total water input were compared (Fig. S8) to reveal the key trends in seasonal changes. It can be seen that during January-April and November-December, the water input was small and snowmelt accounted for a large proportion of the total water

input (more than 80%). As the temperature rose, the rainfall gradually increased, and the snow melted completely in May, accounting for 47%. The importance of snowmelt to winter and spring runoff was highlighted. However, the water input was large from June to September, and rainfall became the main water source. The hydrological process in summer was mainly affected by rainfall.

Furthermore, the relationships between the initial freezing date, last freezing date, and the freezing days of seasonally frozen ground (Fig. S9 (a)), as well as the first snow day, last snow day, and the number of snow cover days (Fig. S9 (b)) were analyzed. The results indicate that the initial freezing date of the soil generally occurred earlier than the snow accumulation date, and the last thawing day was later than the last snow day. This implies that the number of freezing days of the soil exceeds the number of snow cover days. According to the simulation results, the number of soil freezing days remained around 239 days, while the number of snow cover days was approximately 191 days. This reflects the different responses of frozen ground and snow to seasonal changes. Due to the higher heat capacity and slower heat conduction of the soil, the freezing and thawing processes are slower compared to snow. The simulation results also suggested a slight upward trend in both the number of frozen days and snow days during the study period, which is consistent with the existing results (Wu et al., 2024).

Figure Captions

Figure S1. Normalized (a) tension water storage capacity and (b) free water storage capacity distribution.

Figure S2. GXAJ model grid cell: (a) partitioning of runoff sources and (b) soil moisture and evapotranspiration in three soil layers.

Figure S3. Snowmelt process grid cell: (a) runoff components and (b) calculation of soil water/ice content. R_S^* represents surface runoff influenced by frozen ground. W_i^u, W_i^l, W_i^d represent the ice content in the upper, lower, and deep soil layers, respectively, while W_w^d representing the water content in the deep soil layer.

Figure S4. Runoff components of the frozen ground process grid cell. R_S^* and R_I^* represent surface runoff and interflow components influenced by frozen ground.

Figure S5. Soil water/ice content and evapotranspiration of frozen ground process grid cells. $W_i^u, W_i^l,$ and W_i^d represent the ice content in the upper, lower, and deep soil layers, $W_w^u, W_w^l, and\ W_w^d$ represent the water content in the upper, lower, and deep soil layers.

Figure S6. Initial freezing and thawing dates of the surface soil at meteorological stations (a) 56034, (b) 56038, (c) 56146, (d) 56158, (e) 56251, (f) 56167.

Figure S7. Spatial distribution of maximum seasonal frozen ground thickness from (a) the dataset of maximum thickness of seasonally frozen ground from National Tibetan Plateau Data Center, and (b) the model simulation value of this study.

Figure S8. Snow distribution (a) simulated in this study (b) MODIS data, taking December 1, 2015 as an example

Figure S9. The proportion of annual runoff sources simulated during the study period includes rainfall and snowmelt, and the sum of the two is water input.

Figure S10. Trends in the initial date, final date, and number of days for (a) soil freezing and (b) snow cover during the study period.

Table Captions

Table S1. Computational time comparison for the GXAJ, GXAJ-S, and GXAJ-S-SF models.

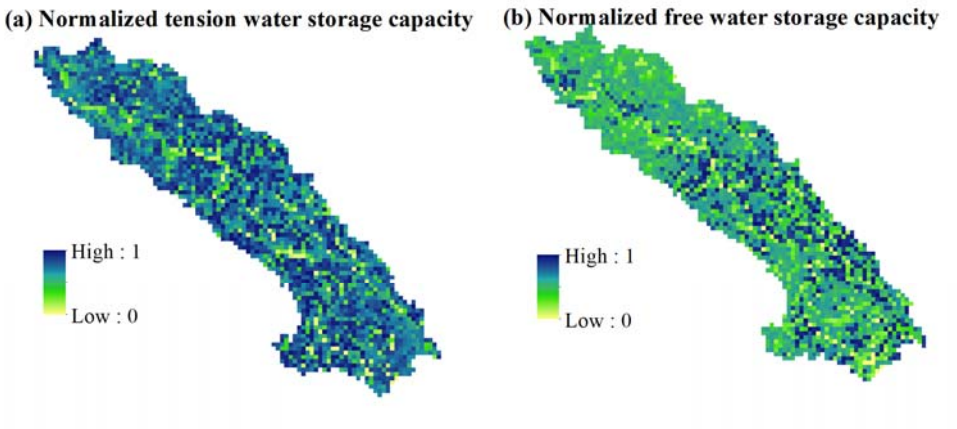

Figure S1. Normalized (a) tension water storage capacity and (b) free water storage capacity distribution.

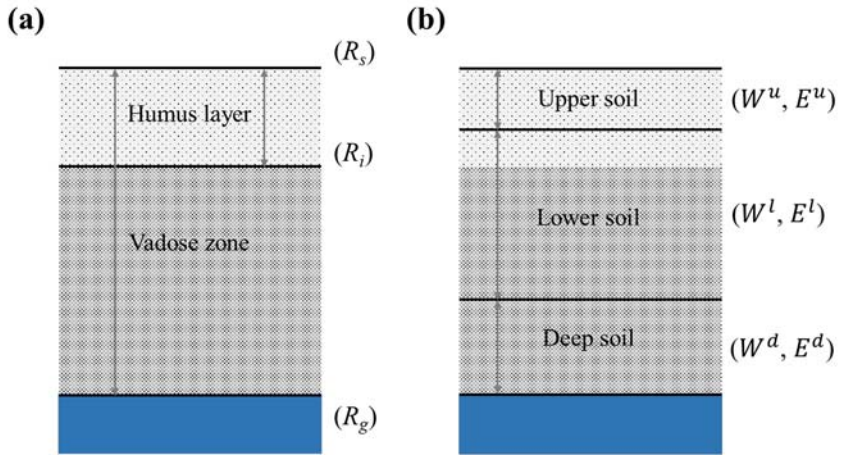

Figure S2. GXAJ model grid cell: (a) partitioning of runoff sources and (b) soil moisture and evapotranspiration in three soil layers.

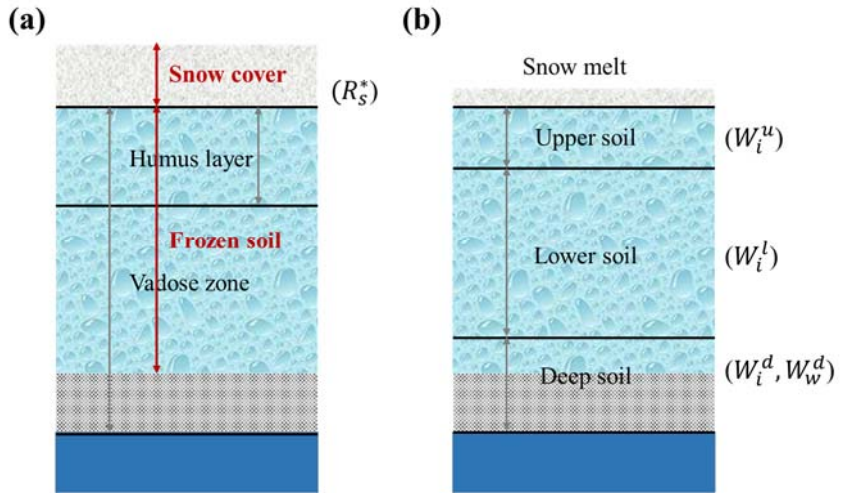

Figure S3. Snowmelt process grid cell: (a) runoff components and (b) calculation of soil water/ice content. R_S^* represents surface runoff influenced by frozen ground. W_i^u, W_i^l, W_i^d represent the ice content in the upper, lower, and deep soil layers, respectively, while W_w^d representing the water content in the deep soil

95 layer.

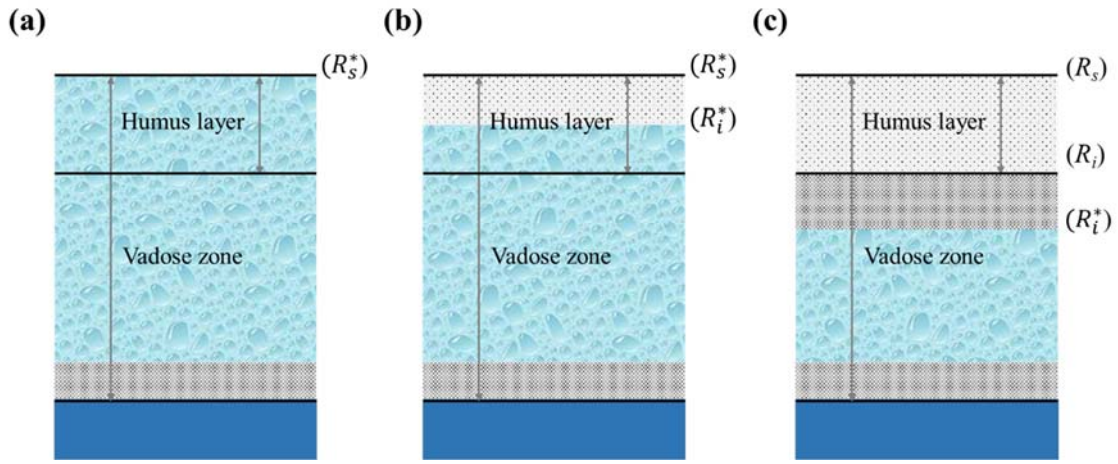

Figure S4. Runoff components of the frozen ground process grid cell. R_s^* and R_i^* represent surface runoff and interflow components influenced by frozen ground.

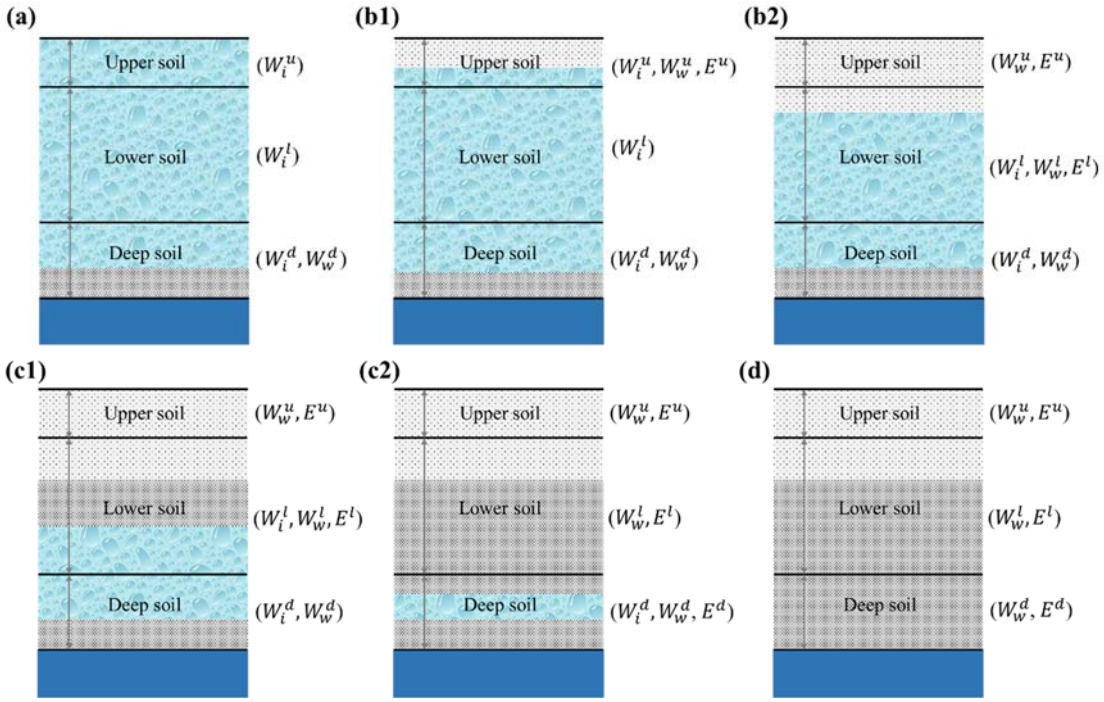

100 **Figure S5.** Soil water/ice content and evapotranspiration of frozen ground process grid cells. $W_i^u, W_i^l,$ and W_i^d represent the ice content in the upper, lower, and deep soil layers, $W_w^u, W_w^l, and\ W_w^d$ represent the water content in the upper, lower, and deep soil layers.

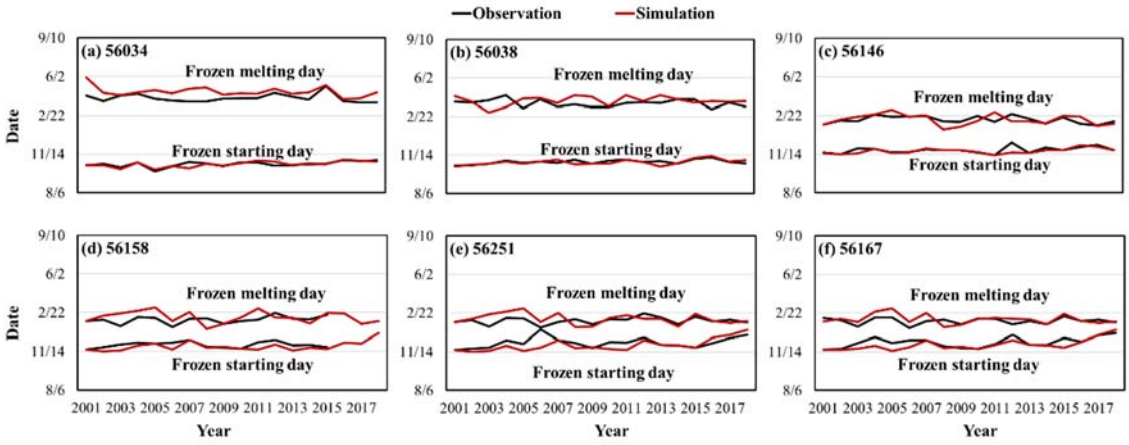

Figure S6. Initial freezing and thawing dates of the surface soil at meteorological stations (a) 56034, (b) 56038, (c) 56146, (d) 56158, (e) 56251, (f) 56167.

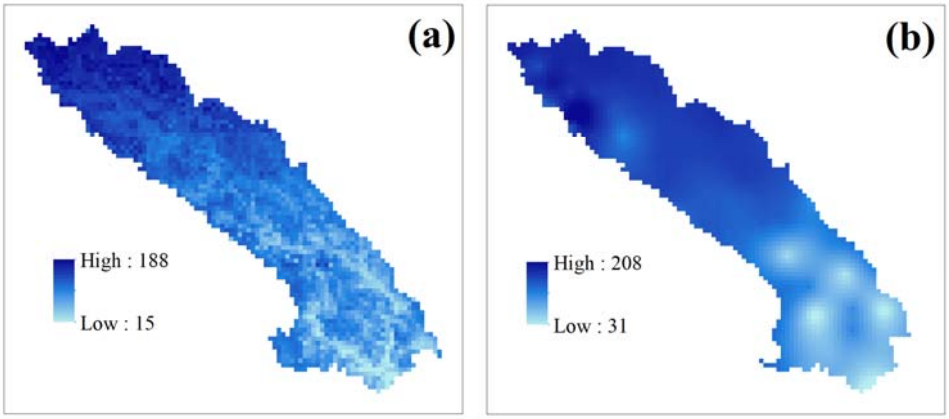

Figure S7. Spatial distribution of maximum seasonal frozen ground thickness from (a) the dataset of maximum thickness of seasonally frozen ground from National Tibetan Plateau Data Center, and (b) the model simulation value of this study.

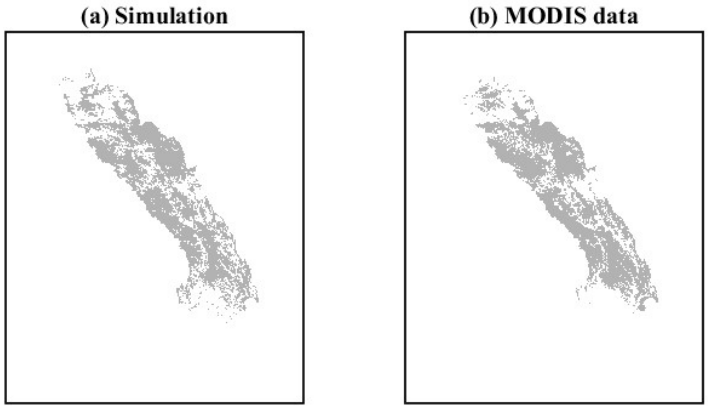

Figure S8. Snow distribution (a) simulated in this study (b) MODIS data, taking December 1, 2015 as an example

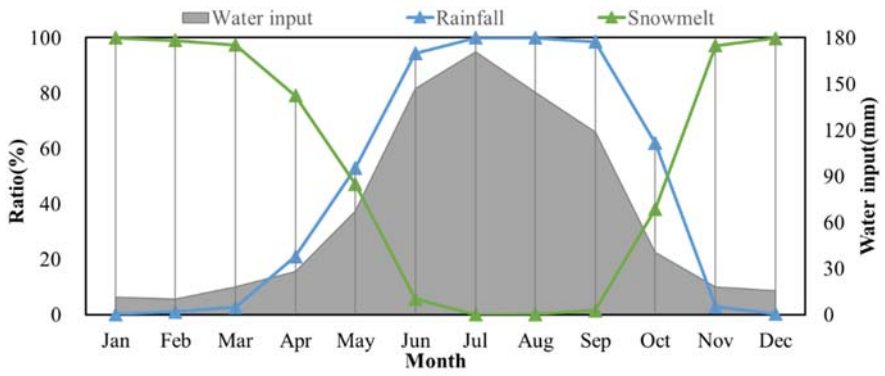

Figure S9. The proportion of annual runoff sources simulated during the study period includes rainfall and snowmelt, and the sum of the two is water input.

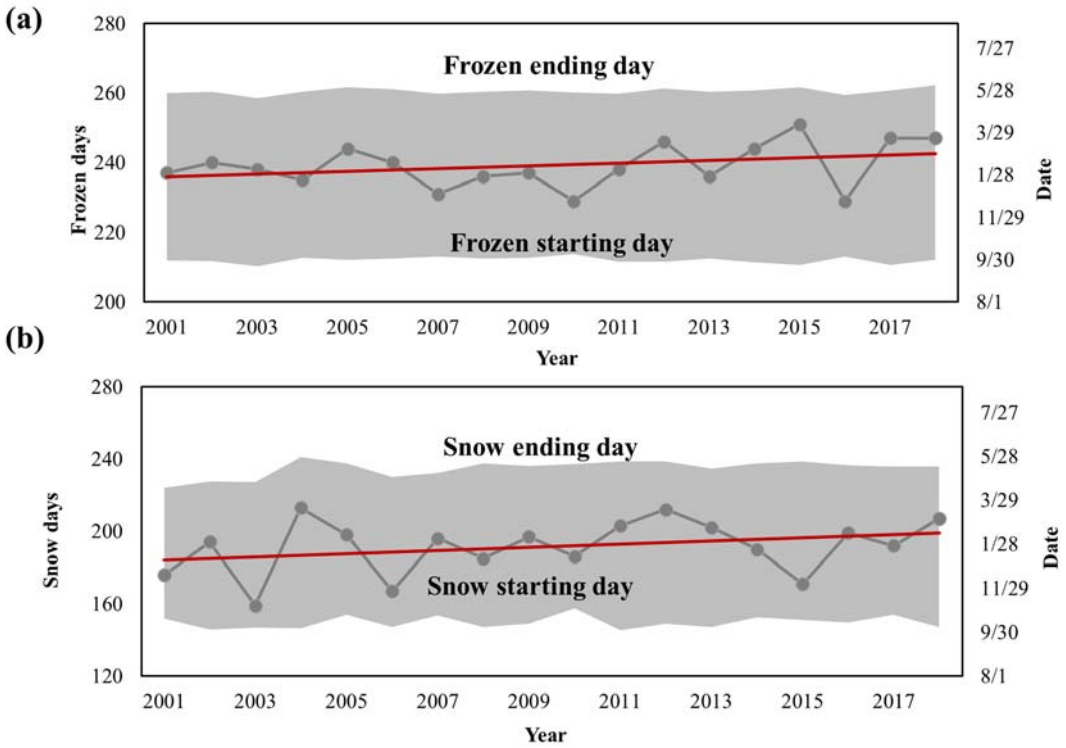

Figure S10. Trends in the initial date, final date, and number of days for (a) soil freezing and (b) snow cover during the study period.

Table S1. Computational time comparison for the GXAJ, GXAJ-S, and GXAJ-S-SF models.

Model	Calibration Time (seconds)	Simulation Time (seconds)
GXAJ	5,422	8.67
GXAJ-S	22232	38.93
GXAJ-S-SF	24294	41.24

 # All simulations were conducted in the following computing environment: AMD Ryzen 5 3600X 6-Core Processor, 32GB DDR4 2133MHz RAM, Windows 10 operating system, and MATLAB R2023a for model implementation and execution. The computations were performed in single-threaded mode, with 400 iterations set for the calibration period.

References

Wu, N., Zhang, K., Chao, L., Ning, Z., Wang, S., & Jarsjö, J. (2024). Snow cover expansion with contrasting depth thinning in the recent 40 years: Evidence from the Yalong River Basin, South-eastern Tibetan Plateau. *Journal of Hydrology: Regional Studies*, *53*, 101786. https://doi.org/10.1016/j.ejrh.2024.101786